A holistic modeling framework for estimating the influence of climate change on indoor air quality

Salthammer, Tunga

2022-06

Salthammer , T , Zhao , J , Schieweck , A , Uhde , E , Hussein , T , Antretter , F , Künzel , H , Pazold , M , Radon , J & Birmili , W 2022 , ' A holistic modeling framework for estimating the influence of climate change on indoor air quality ' , Indoor Air , vol. 32 , no. 6 , e13039 . https://doi.org/10.1111/ina

http://hdl.handle.net/10138/347796
https://doi.org/10.1111/ina.13039

Received: 2 January 2022 | Revised: 22 April 2022 | Accepted: 2 May 2022

DOI: 10.1111/ina.13039

ORIGINAL ARTICLE

WILEY

A holistic modeling framework for estimating the influence of climate change on indoor air quality

Tunga Salthammer[1] | Jiangyue Zhao[1] | Alexandra Schieweck[1] | Erik Uhde[1] | Tareq Hussein[1,2,3] | Florian Antretter[4,5] | Hartwig Künzel[4] | Matthias Pazold[5] | Jan Radon[5,6] | Wolfram Birmili[7]

[1]Department of Material Analysis and Indoor Chemistry, Fraunhofer WKI, Braunschweig, Germany

[2]University of Helsinki, Institute for Atmospheric and Earth System Research (INAR), Helsinki, Finland

[3]School of Science, Department of Physics, Environmental and Atmospheric Research Laboratory (EARL), University of Jordan, Amman, Jordan

[4]Department Hygrothermics, Fraunhofer Institute for Building Physics (IBP), Valley, Germany

[5]C3RROlutions GmbH, Raubling, Germany

[6]Faculty of Environmental Engineering, University of Agriculture in Krakow, Krakow, Poland

[7]Department II 1 "Environmental Hygiene", German Environment Agency (Umweltbundesamt), Berlin, Germany

Correspondence
Tunga Salthammer, Fraunhofer WKI, Department of Material Analysis and Indoor Chemistry, Bienroder Weg 54 E, 38108 Braunschweig, Germany.
Email: tunga.salthammer@wki.fraunhofer.de

Funding information
Federal Ministry for the Environment, Nature Conservation, Nuclear Safety and Consumer Protection (BMUV): REFOPLANFKZ3719512050

Abstract

The IPCC 2021 report predicts rising global temperatures and more frequent extreme weather events in the future, which will have different effects on the regional climate and concentrations of ambient air pollutants. Consequently, changes in heat and mass transfer between the inside and outside of buildings will also have an increasing impact on indoor air quality. It is therefore surprising that indoor spaces and occupant well-being still play a subordinate role in the studies of climate change. To increase awareness for this topic, the Indoor Air Quality Climate Change (IAQCC) model system was developed, which allows short and long-term predictions of the indoor climate with respect to outdoor conditions. The IAQCC is a holistic model that combines different scenarios in the form of submodels: building physics, indoor emissions, chemical–physical reaction and transformation, mold growth, and indoor exposure. IAQCC allows simulation of indoor gas and particle concentrations with outdoor influences, indoor materials and activity emissions, particle deposition and coagulation, gas reactions, and SVOC partitioning. These key processes are fundamentally linked to temperature and relative humidity. With the aid of the building physics model, the indoor temperature and humidity, and pollutant transport in building zones can be simulated. The exposure model refers to the calculated concentrations and provides evaluations of indoor thermal comfort and exposure to gaseous, particulate, and microbial pollutants.

KEYWORDS
building simulation model, emission rates, exposure, gas-phase reactions, indoor aerosol model, mold growth

1 | INTRODUCTION

In addition to population growth and the pollution of ecosystems, climate change as a result of anthropogenic greenhouse gas emissions is the greatest challenge of our time. Current forecasts predict an average global temperature increase of 1.4–4.4°C by the end of the 21st century, depending on the specific scenario.[1] In addition, significant warming of the air over the continents, a rise in sea level, and melting of the sea ice are expected. Since the 19th century, mean temperatures in Germany have risen by an annual average

of +1.3°C.[2] Based on the medium SSP2-4.5 scenario (SSP =Shared Socioeconomic Pathways), which assumes a greenhouse gas concentration of 650 ppm and a radiative forcing value of 4.5 W/m² by 2100,[1] a permanent increase in the average temperatures and the number of hot days and more extreme weather events are expected in Central Europe.[2] Changes in moisture content and the rates of photochemical reactions will also affect the atmosphere, which can lead, for example, to the increased formation of ozone and particulate matter.[3] The *"actio-reactio"* principle between man and planet is particularly fatal. Human action changes the climate in a very short time, and answers come in the form of extreme weather, which in turn changes the organization of society and their way of life.

The conditions of outdoor air associated with climate change have a direct impact on people's living environment.[4] Temperature, water balance, and direct solar radiation will increasingly affect the building fabric and consequently indoor air quality and the well-being of dwellers. People in urban societies spend about 80%–90% of their time in various types of private and public indoor environments.[5,6] Consequently, exposure indoors is of the highest relevance with regard to preventive health care against climatic influences.

Nazaroff[7] assumes a rise of indoor pollution and exposure if the concentration of chemicals in outdoor air increases. In addition, highly insulated but manually ventilated buildings may overheat in the warm season, which can lead to a trend toward the use of air conditioning systems. Nazaroff[7] and Spengler[8] therefore expect a possible increase in energy consumption and more device-specific emissions in the future. One approach to take climate change into account is to use well-planned and constructed building envelopes that are equipped with effective ventilation and filter technologies.[7,9]

The Institute of Medicine (IOM)[10] views children, the elderly and sensitive population groups under a particular health risk as a result of climate change. In cities with a high population density and high traffic volume, the effects of anthropogenic outdoor air pollutants such as nitrogen oxides (NO_x) and particulate matter (PM_{10} and $PM_{2.5}$) are already noticeable and have an impact on indoor air quality.[11] In particular, heat waves will have an increasingly negative effect on indoor conditions.[12–16] In most parts of Europe, heat waves are still seen as unusual occurrences, although experience has changed in recent years.[17–20] In other parts of the world, for example Australia, high outdoor air temperature is not uncommon.[21,22] It can be assumed that buildings will heat up more in the future, especially in urban areas and as a result of the densification of settlement areas.[23] In the interior, temperature, and humidity, the release of air pollutants and their possible chemical reactions in the room air will become just as important as the risk of mold formation on building surfaces.

In view of these developments, it is necessary to obtain more accurate and precise knowledge about the effects of rapidly changing conditions in outdoor areas on the indoor environment. It therefore seems sensible and important to develop a model system that, on the basis of computer-aided simulations, allows a forecast of indoor air quality over different scenarios in the coming decades. Currently, it is hardly possible to estimate specific consequences on the basis of the available scientific studies. Previous work has mainly focused on individual aspects that influence climatic parameters and pollutant concentrations in indoor spaces. Numerical model systems that have already been developed for heat and moisture transport[24] and chemical processes[25] are linked to one another for the relevant influencing factors and boundary conditions. The merging of different approaches leads to the holistic IAQCC (Indoor Air Quality Climate Change) model system.

Practical implications

- A modeling system is being developed to predict indoor air quality and exposure under the influence of different climate change scenarios in the coming decades.
- The model simulates indoor heat and moisture transport, indoor gas and particle concentrations, the risk of mold growth, and relevant indoor chemical–physical processes.
- The results of the short-term and long-term calculations provide a basis for future thermal insulation and ventilation strategies.

2 | MODEL ARCHITECTURE AND OBJECTIVES

The IAQCC model presented here (see Figure 1) was designed to simulate indoor climate and air quality as a function of building parameters, residential activities, and ambient conditions. The model combines various submodels for building physics (particularly considering the heat and moisture transfer as well as air exchange), gaseous and particulate emissions from indoor sources, gaseous chemical reactions, gas-phase/particle-phase partitioning, aerosol particle dynamics, mold growth and estimating residents' comfort and cumulative pollutant exposure. These modules are described in detail below.

The IAQCC model is initialized with a physical configuration of a single-family home. Model simulations are driven by time-resolved ambient meteorological parameters, prescribed by a selection of climate change scenarios. Residential activities such as ventilation and source activities are included in the simulations at high time resolution.

The output of the IAQCC model allows quantitative estimates as well as sensitivity studies on how climate change can affect indoor air climate and air quality. These data will help formulate suitable measures and recommendations on how to deal with and adapt to changing environmental conditions. Our first simulations were performed for the specific climate and an anticipated climate change in Germany although corresponding future work can provide results for any region of the globe.

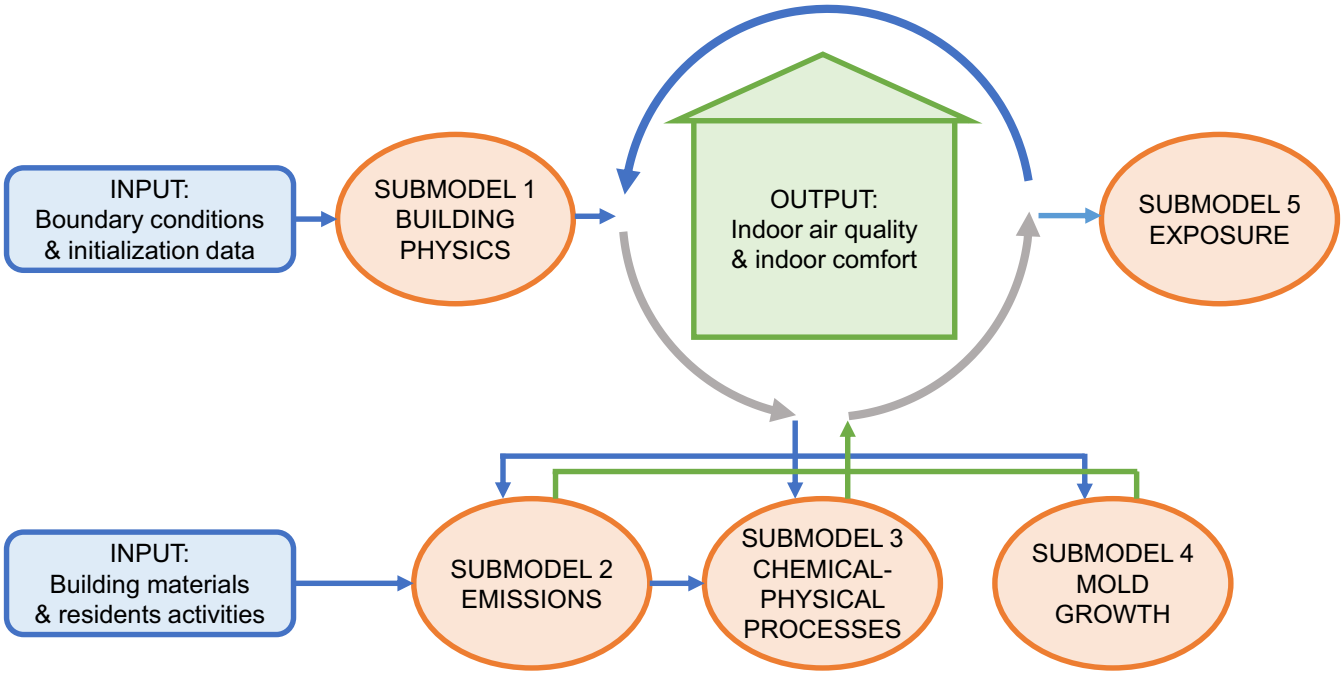

FIGURE 1 IAQCC model architecture. The five submodels are marked in orange circles. Blue color represents data input; green color represents data output of the respective submodels

TABLE 1 Chemical properties of the target compounds

Compound	CAS-No.	MW[d] (g/mol)	BP[d] (°C)	P_0[e] (Pa)	log K_{OW}[f]	H[g] mol/(m³·Pa)	log K_{OA}[h]
Limonene	138-86-3	136.2	176.0	$2.2{\cdot}10^{2}$	4.57	$4.8{\cdot}10^{-4}$	4.32
Isoprene	78-79-5	68.1	34.0	$7.3{\cdot}10^{4}$	2.42	$3.4{\cdot}10^{-4}$	2.03
Formaldehyde	50-00-0	30.0	−19.1	$5.2{\cdot}10^{5}$	0.35	$3.5{\cdot}10^{1}$	1.37
n-Butyl acetate	123-86-4	116.2	126.1	$1.5{\cdot}10^{3}$	1.78	$2.1{\cdot}10^{-2}$	3.88
n-Decane	124-18-5	142.3	174.1	$1.9{\cdot}10^{2}$	5.05	$2.1{\cdot}10^{-6}$	4.03
Acetic acid	64-19-7	60.1	117.9	$2.1{\cdot}10^{3}$	−0.17[i]	$4.0{\cdot}10^{1}$	3.54
Acetaldehyde	75-07-0	44.1	20.1	$1.2{\cdot}10^{5}$	−0.34	$1.3{\cdot}10^{-1}$	1.98
Toluene	108-88-3	92.1	110.6	$3.8{\cdot}10^{3}$	2.73	$1.5{\cdot}10^{-3}$	3.31
Benzophenone	119-61-9	182.2	305.4	$1.5{\cdot}10^{-1}$	3.18	6.1	7.23
TEP[a]	78-40-0	182.2	215.5	$5.2{\cdot}10^{1}$	0.80	$2.7{\cdot}10^{2}$	5.21
TXIB[b]	6846-50-0	286.4	280	$3.0{\cdot}10^{-1}$	4.38	$1.8{\cdot}10^{-1}$	9.71
DEHA[c]	103-23-1	370.6	417.0	$8.4{\cdot}10^{-6}$	6.85	1.4	10.80

[a]TEP, Triethyl phosphate.
[b]TXIB, 2,2,4-Trimethyl-1,3-pentanediol diisobutyrate.
[c]DEHA, Di-2-ethylhexyl adipate.
[d]Data from PubChem (https://pubchem.ncbi.nlm.nih.gov/).
[e]Data (298 K) from PubChem (https://pubchem.ncbi.nlm.nih.gov/). P_0 for benzophenone (subcooled liquid) from Sejfa et al.,[26] P_0 for TXIB calculated from SPARC.
[f]Data (298 K) from PubChem (https://pubchem.ncbi.nlm.nih.gov/), log K_{OW} for TXIB calculated from SPARC, log K_{OW} for DEHA from Salthammer et al.[27]
[g]Data (298 K) from Sander.[28] H for TXIB calculated from SPARC.
[h]Data (298 K) from Baskaran et al.,[29] log K_{OA} for benzophenone and TXIB calculated from SPARC, log K_{OA} for DEHA from Salthammer et al.[27]
[i]Note that acetic acid ionizes in water (pK_s 4.76).

Organic compounds play a central role in indoor air quality assessment because they are ubiquitous in building components, furniture, lifestyle products, and even ambient air. Due to the large number of organic compounds potentially occurring indoors, a selection was made to represent some major compound classes and a range of health-relevant compounds. The relevant volatility range of VVOCs, VOCs, and SVOCs (very volatile, volatile, and semi-volatile organic compounds) with regard to boiling point (BP) and vapor pressure (P_0)

were taken into account. The affinity for polar or non-polar media, expressed by the octanol/water partition coefficient K_{OW}, the Henry constant H, and the octanol/air partition coefficient K_{OA}, can be assumed to vary widely. Finally, substances can be assumed reactive or inert under indoor conditions. The 12 selected compounds and their physical properties are listed in Table 1.

3 | MODEL DESCRIPTION

3.1 | Building physics model (Submodel 1)

The building physics model is a multi-zone hygrothermal whole building simulation model as described by Antretter et al.,[30,128] which has been used worldwide and extensively validated. It computes the heat and moisture balance of the building zones and serves as the orchestrator of the submodels described in Sections 3.2–3.6. The baseline for the calculation of the air temperature (θ_i) in the i-th zone and relative humidity (ϕ_i) in the same zone is the enthalpy and moisture balance of the respective zone. These balances consider fluxes across enclosing surfaces (opaque and transparent), through natural/mechanical ventilation equipment-induced air exchange as well as interior heat and moisture sources/sinks. The specific enthalpy is related to 1 kg of dry air and is by definition 0 kJ/kg at $T = 273.15$ K and standard pressure.[31] The model also allows evaluating the conditions of the building envelope, which has a significantly higher heat transfer coefficient than the surrounding areas, resulting in lower surface temperatures. These areas are also known as thermal bridges.[32] Figure 2 shows a simplified visualization of heat and moisture fluxes considered in the balances.

The change of total enthalpy in zone i, dH_i in Joule, according to equation (1) is a result of the transmission heat flow through n enclosing building components $\dot{Q}_{Comp}$, solar gains $\dot{Q}_{Sol}$ through n windows or transparent components, the contribution of n interior convective heat sources $\dot{Q}_{Int}$, ventilation heat flow $\dot{Q}_{Vent}$ via n air-flow path and the convective heat source or sink $\dot{Q}_{HVAC}$ due to n HVAC (heating, ventilation, and air conditioning) equipment elements, all in Watt.

$$\frac{dH_i}{dt} = \sum_{j=1}^{n} \dot{Q}_{Comp,j} + \sum_{j=1}^{n} \dot{Q}_{Sol,j} + \sum_{j=1}^{n} \dot{Q}_{Int,j} + \sum_{j=1}^{n} \dot{Q}_{Vent,j} + \sum_{j=1}^{n} \dot{Q}_{HVAC,j} \quad (1)$$

It is important to note that the total enthalpy in zone i depends on the specific enthalpy of the air in that zone. This specific enthalpy of moist air is the sum of the enthalpy of dry air and the moisture content-related enthalpy of vapor. As a result, the enthalpy zone balance depends on the moisture balance of the zone as described in equation (2) and both zone balances can only be solved iteratively.

$$\frac{dM_i}{dt} = \sum_{j=1}^{n} \dot{W}_{Comp,j} + \sum_{j=1}^{n} \dot{W}_{Int,j} + \sum_{j=1}^{n} \dot{W}_{Vent,j} + \sum_{j=1}^{n} \dot{W}_{HVAC,j} \quad (2)$$

The change of total moisture content in zone i, dM_i in kg is a result of moisture flow through n enclosing building components $\dot{W}_{Comp}$, n interior moisture sources $\dot{W}_{Int}$, ventilation-based moisture flow $\dot{W}_{Vent}$, and moisture addition or removal through HVAC equipment $\dot{W}_{HVAC}$, with all flows in kg/s.

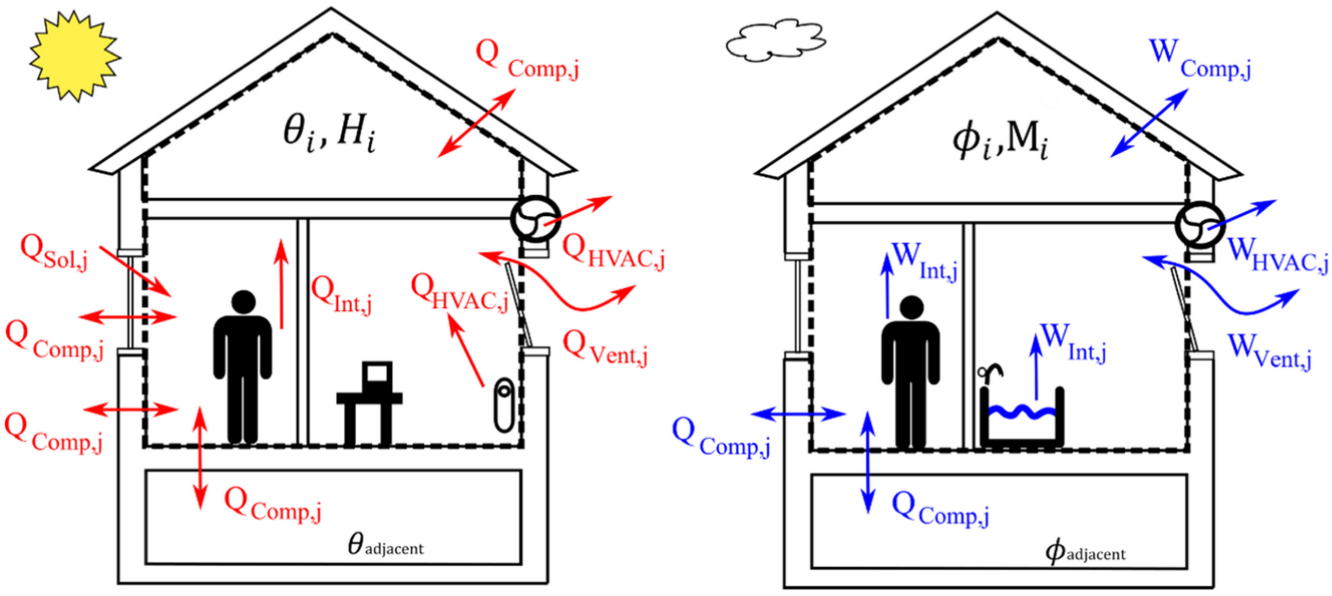

FIGURE 2 Simplified visualization of the balances of heat and moisture fluxes in a building zone to compute the total zone enthalpy H_i according to equation (1) and the total moisture content M_i of the zone according to equation (2) with heat flow through n enclosing building components $\dot{Q}_{Comp}$; solar gains $\dot{Q}_{Sol}$; internal heat sources $\dot{Q}_{Int}$; ventilation heat flow $\dot{Q}_{Vent}$; HVAC equipment heat source or sink $\dot{Q}_{HVAC}$; moisture flow through n enclosing building components $\dot{W}_{Comp}$; interior moisture sources $\dot{W}_{Int}$; ventilation moisture transport $\dot{W}_{Vent}$; HVAC equipment moisture source or sink $\dot{W}_{HVAC}$

The coupled heat and moisture transport in building components is calculated according to Künzel.[24] Transparent building components consider transmission loss via an overall U-value and solar gains via an angular-dependent solar heat gain coefficient which considers direct and diffuse radiation accordingly. The total air exchange rate and ventilation-based flow is a result of solving an air-flow network,[33] which considers air exchange between the zone and other zones as well as with the outside, all of which can come with different enthalpy, moisture content, and gas and particle concentrations. It is separated into infiltration, natural ventilation, and mechanical ventilation, with the latter also being able to account for heat/enthalpy recovery. The separate ventilation components come with different penetration factors as described in Section 3.3. The use of a building generates heat and moisture sources. People and equipment can emit heat through radiation, which affects the surface nodes of the enclosing components, and convection as well as moisture. To maintain set points for temperature and humidity in the zones, a HVAC equipment is used in the building physics model that immediately heats, cools, humidifies, and dehumidifies the space if the setpoints are not met.

3.2 | Emission model (Submodel 2)

In residential indoor environments, organic and inorganic compounds as well as particles can be released into indoor air from building materials, furniture, and various occupant activities. As shown in Figure 1, these indoor sources are treated separately in two groups in the emission model due to differences in emission mechanism and pattern. The first emission group is building materials, including floor coverings (e.g., laminate, carpet, and PVC), wall coatings (e.g., plaster and wallpaper), and furniture (e.g., wood-based materials, textiles, and foams). It is important to note that depending on their physicochemical properties, they can serve as both a source and a sink. The second group represents emissions from indoor activities such as cooking, cleaning, lighting candles, other combustion processes and using electronic equipment, which are often short source episodes but cause large increases in pollutant concentrations.

For emissions from building materials, two types of models are commonly used to quantify the emission: the mass transfer model and the empirical model. The mass transfer model is a physically based diffusion model which includes several controlling factors, for example, initial concentration of a VOC in the material, the diffusion coefficient, and the material/air partition coefficient.[34–36] However, different estimation methods and indoor conditions for these control factors may have large discrepancies, a simple and accurate estimation method for different materials is not yet available.[37–39] The empirical model predicts the emission behavior over time by nonlinear regression analysis[40] of the experimental data (e.g., first-order exponential, double-exponential, and power-law decay curve).[41,42] Strictly speaking, the data measured in this way can only be used for the respective experimental conditions. However, results on emissions under different conditions (temperature, humidity, air exchange, loading) are available for a large number of substances and products. It is also possible to combine the results of both models, for example with temperature-dependent emission rates.[43,44] The IAQCC model adapts empirical modeling approaches using available datasets for furniture, building products and consumer products. Area-specific and unit-specific emission rates are provided depending on the type of source and allow the user to design the desired room furnishings. The change in emission rate as a function of temperature is also considered. The influence of air humidity is taken into account if necessary. This is particularly important for formaldehyde emissions from wood-based materials and appropriate modeling tools are available here.[45] Another case concerns the degradation of organic esters. However, it might be difficult to distinguish between biotic and abiotic processes.[46]

To account for influences of ambient air and emissions from activities, the emission model was developed on the basis of a mass-balance approach, in which the change in indoor pollutant concentrations is controlled by outdoor infiltration, exfiltration, indoor sources, and sinks (see Figure 3). An emission database for indoor gas and aerosol particle emissions in European households was created through analyzing data from the literature. Particle concentrations and sources were characterized using data from a 2016 – 2019 measurement campaign of 40 homes in Germany.[48] The data include particle number size distribution (PNSD, particle size 10–800 nm) and activity patterns (source type, frequency, and duration) of occupants in real-use dwellings.[47–49] With the aid of the extended indoor aerosol model (IAM model) developed for this work (see Section 3.3), particle emission rates with detailed size information were calculated and identified for more than 500 known indoor source events. More data on sources of airborne particles and gas-phase pollutants are available for combustion processes,[50–54] cooking,[55,56] use of office equipment,[57–60] cleaning and many other types of activities[61–65] from additional studies and reviews. Dimitroulopoulou et al.[66–68] conducted a Europe-wide study on emissions from the use of consumer products (EPHECT, Emissions, exposure Patterns and Health Effects of Consumer products in the EU), which can be used to assess the indoor key pollutants emission strength and pattern from these products.

3.3 | Chemical–physical model (Submodel 3)

The chemical–physical model focuses on the key processes in the indoor environment from the aspect of mass transfer including aerosol dynamics and gas-phase reactions (see Figure 3). Hussein and colleagues[69–71] have developed the IAM model to simulate time-evolving size-resolved indoor particle dynamics, including ventilation, outdoor penetration, indoor particle deposition, and coagulation losses. To better describe the evolution of indoor particles due to coagulation, the IAM model was further developed in this work. In each simulation timestep, the PNSD changes while maintaining the overall mass balance, that is, the mass loss of the small particles through collisions is equal to the mass gain of the corresponding

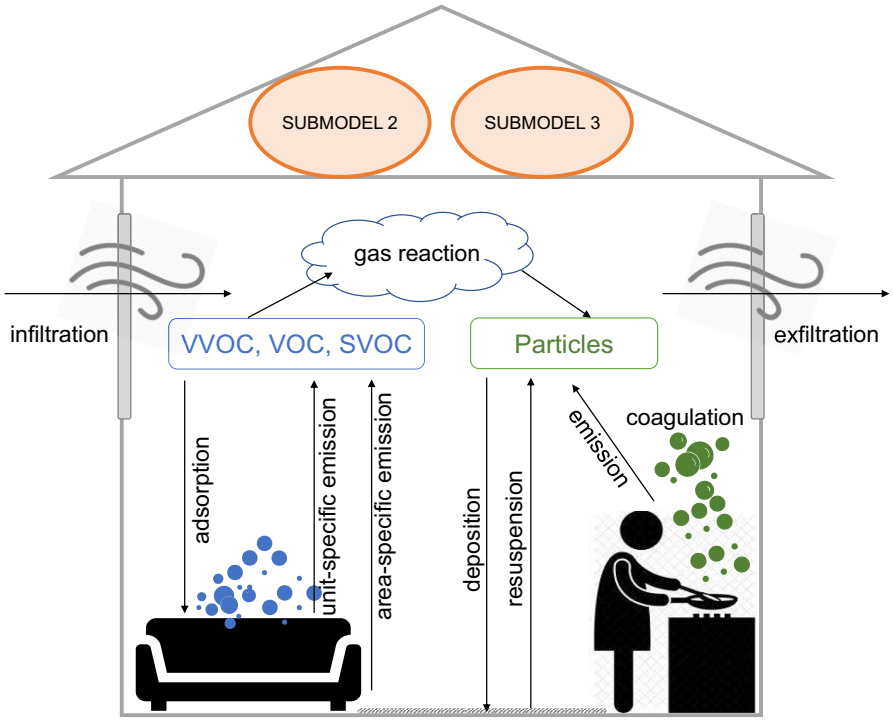

FIGURE 3 Mass transfer and chemical processes involved in the IAQCC model

larger particles. To correctly respond to influences of climate change, the fundamental parameters in the deposition and coagulation model were introduced as a function of temperature instead of a constant value, including dynamic viscosity, air density, and mean free path of the molecules of the air.

The model of gas-phase reaction was developed based on the well-established comprehensive Master Chemical Mechanism (MCM, v3.3.1).[72] The model deals with the degradation of 142 substances of the VOCs group and simulates the formation of hydroxyl (OH) radicals in indoor air, which contribute to the formation of so-called secondary organic aerosols (SOA). The model includes thousands of different reactions and individual substances. To facilitate model development and limit computational resources, this work employs a version of MCM that uses a limited set of substances and reactions—particularly such that involve relevant rate constants for ozone and the OH radical.

The formation of SOA from atmospheric reactions has been widely studied.[73] It became clear that it is impossible to assign a general formation yield for SOA to a certain reaction type, since this depends on various factors such as the background concentration of aerosols and temperature.[74] Different values have even been published for the later discussed (see Section 4.4) and previously well-studied example of limonene/O_3/OH.[75–77] Youssefi and Waring[78] found that the yields of terpene ozonolysis are highly variable indoors and that literature data can be uncertain. Nevertheless, estimations of newly formed aerosol particles are included in the IAM model and follow the particle dynamic simulation. It must also be taken into account that SVOCs tend to adsorb to different indoor surfaces and particles due to their low volatility.[79,80] Based on previous works, the ratio between a substance sorbed to airborne particles and in the gas phase can be quantified by the particle/gas partition coefficient (K_p) and the total suspended particle concentration [TSP].[81–83]

$$\frac{F}{C_g} = [\mathrm{TSP}] \bullet K_p \tag{3}$$

F and C_g are the particle-phase and gas-phase concentrations of the substance, respectively. Rearrangement of equation (3) gives the proportion of molecules in the particle phase Φ.

$$\Phi = \frac{F}{C_g + F} = \frac{K_p \bullet [\mathrm{TSP}]}{1 + K_p \bullet [\mathrm{TSP}]} \tag{4}$$

The general equation of the emission model and chemical–physical mode is described as follows:

$$\frac{dC_i}{dt} = P \bullet \lambda \bullet C_e - \lambda \bullet C_i - \lambda_d \bullet C_i + \sum_{j=1}^{n} \frac{\mathrm{SER}_{A,j} \bullet A_j}{V} + \sum_{j=1}^{n} \frac{\mathrm{SER}_{u,j}}{V} \pm J_{coag} \pm \xi \bullet \psi_{gas} \pm J_{SVOC} \tag{5}$$

C_i and C_e are the indoor and outdoor concentrations of the target size particle or target gas species (#/cm^3 or µg/m^3), respectively. P is the outdoor penetration factor, λ is the air exchange rate (h^{-1}), and λ_d is the deposition rate of particles or a gas species on indoor surfaces (h^{-1}). The emission rate SER of a specific source j is represented as either area-specific $\mathrm{SER}_{A,j}$ in µg/(m^2·h) or as unit-specific $\mathrm{SER}_{u,j}$ in µg/h for gas-phase species and #/h for particles). A_j is the area of emission source in m^2, and V is the room volume in m^3. J_{coag} is the coagulation term for gain or loss of the target size particle.

$\psi_{gas} = k_{[gas][ox]} \bullet C_g \bullet C_{ox}$ is the production or removal rate of a species due to gas-phase chemistry, where $k_{[gas][ox]}$ is the reaction rate constant for reactive organic gases and oxidant (ox), C_{ox} is the concentration of the oxidant. In equation (5), $\xi = 1$ for the gas-phase balance.

In the particle-phase balance, ξ represents the SOA yield, $\xi \bullet \psi_{gas}$ is thus the amount of SOA obtained from the corresponding gas reaction. The last term J_{SVOC} is relevant when the target compound is an SVOC, which describes the SVOC loss as gas phase and gain as particle phase. Taking C_i as the gas-phase concentration (analogous to C_g) of the target SVOC in equation (5), the fraction of a compound sorbed on airborne particles (F) can thus be estimated according to equation (3).

3.4 | Mold growth model (Submodel 4)

Indoor mold and moisture, and their associated health effects, are a society-wide problem. The evaluation of the mold risk in buildings is therefore instrumental to access a healthy environment. Several advanced models are available for predicting mold on surfaces of building elements.[84] Most of these models use the main factors that influence mold growth—the temperature and relative humidity (or water activity) on the surface under consideration and the exposure time—to experimentally derive correlations which also lead to shortcomings.[85] For the IAQCC model system, two of the most widely used mold models were considered: The Sedlbauer bio-hygrothermal model,[86] which is a semi-physical model, and the VTT (Technical Research Centre of Finland) mold model[87] in its improved version,[88] which is an empirical model.

The bio-hygrothermal model aims to simulate the moisture balance of a mold spore. In combination with temperature and humidity-dependent isopleth systems (for three substrate groups), spore germination and mycelium growth are evaluated. Since the basic substrate groups—non-compostable, compostable, and nutrient materials—are quite coarse, measured isopleths for materials of interest may be added to the model. The VTT model is based on laboratory measurements that can also handle transient boundary conditions and considers a decline, for example in periods of low humidity or below zero temperatures. It is the method of choice for mold assessment according to ASHRAE SPC 160.[89,90] The model provides a mold growth index with six categories. While the two models are quite different, the calculated growth in mm from the bio-hygrothermal model corresponds to the VTT mold index.[91]

Both models are usually used as post-processing modules, that is, the resulting transient surface temperature and relative humidity conditions are fed into the mold modules after simulation, where the mold index and mycelial growth in mm are calculated, respectively. For the IAQCC model system, the approach is further developed to evaluate the change in mold growth risk for every simulation timestep and provide the information back to the zone model. This allows control of the influencing indoor environmental parameters and the ventilation rates based on the mold risk.

3.5 | Exposure model (Submodel 5)

Comfort and human exposure to environmental pollutants are evaluated from the model simulations considering differing boundary conditions and various climate change scenarios. This includes thermal comfort, the inhalation of gaseous substances and particles, the deposition of particles in the lungs, and the potential exposure to microorganisms. The expected discomfort can be calculated on the basis of the discomfort index (DI) as introduced by Thom.[92] The Thom index is a physiological thermal stress indicator considering dry-bulb T_d and wet-bulb temperature T_w. Equation (6) presented by Epstein and Moran[93] for the Celsius scale is a modification of the relationship originally formulated by Thom for Fahrenheit.

$$DI = 0.4 \bullet (T_d + T_w) + 8.3 \quad (6)$$

DI is obtained by using modeled data for temperature and relative humidity indoors from the building physics submodel, T_w can be calculated from the air temperature and the relative humidity.[94] Below a DI of 22 there is no thermal discomfort, but heat stress is becoming serious at DI >28.[93] An alternate method to calculate thermal stress (not discussed here) is the wet-bulb globe temperature index (WBGT) according to ISO 7243.[95]

In addition to thermal comfort, the IAQCC model also targets on the assessment of exposure by inhalation to indoor air pollutants and will be applied both to gaseous substances and particle concentrations. Regarding the model room(s), gas and particle concentrations as well as their lifespan will be calculated. The breathing rate and thus the air intake depends on the physical constitution and the activity level.[71,96,97]

Submodel 3 provides particle size distribution data. In combination with a human respiratory tract model, which was originally developed by the International Commission on Radiological Protection (ICRP),[98] the particle deposition dose in five different regions of the respiratory tract can be modeled: ET1, extrathoracic region 1, consisting of anterior nose; ET2, extrathoracic region 2, including inner nostrils, larynx, throat, and mouth; BB: bronchial region, consisting of the trachea and bronchi; bb, bronchiolar region, consisting of bronchioles and terminal bronchioles; AI: Alveolar-interstitial region, consisting of respiratory bronchioles, alveolar ducts and sacs with their alveoli, and the interstitial connective tissue.[99] In order to simplify the obtained results, ET1 and ET2 will be combined to one ET region, BB and bb will be summarized as BB/bb region.

3.6 | Operating the combined IAQCC model

Each of the five submodels described in Section 3.1–3.5 allows performing standalone calculations. However, to achieve a holistic IAQCC picture, these submodels are operated alongside, thereby interacting and exchanging information as shown in Figure 4.

The building physics module is the simulation master and is responsible for getting and setting information to the submodels and handling of the simulation timesteps. In general, there are two approaches to numerically approximate the time-dependent physical processes—the implicit and the explicit method. Implicit calculation means repeating a timestep with adjusted time-varying values until convergence to arrive at the current state. The explicit method

calculates directly by adjusting the variables for the next timestep and the next system state. A decision criterion for the selection of the method is the timestep size, the time granularity. To ensure a stable calculation process, the explicit scheme usually requires much smaller timesteps than the implicit scheme. For the model system that includes the emission and the chemical–physical model, short timesteps (i.e., one minute or less) are required. The timestep of one hour typically used in building simulation would smooth out rapid changes in concentrations and is therefore too long. Thus, for the holistic IAQCC model, the explicit method is chosen. The building physics model adjusts its global timestep size mostly according to the agile air-flow/ventilation model. The submodels can follow these global timestep sizes or use their own independent timesteps. However, their input data, for example, boundary conditions, like indoor climate and ventilation rates are calculated by the building physics model at each global timestep. This means, they may use smaller timesteps for internal calculations but return their results to the master algorithm at the global timestep.

4 | APPLICATION OF THE SUBMODELS

To visualize the capability and performance of the IAQCC model components, exemplary simulations are presented while applying the various submodels. The discussion of chemical compounds focuses on those listed in Table 1. If possible, the results of the simulations were compared with experimental data.

4.1 | Simulation of temperature and humidity in a building during summer

A key feature of the IAQCC model is the calculation of realistic indoor temperature and relative humidity driven by ambient meteorological data from weather stations. For validation purposes, experimental room temperature and relative humidity data were continuously recorded as 30-minute means using a data logger (Rotronic Messgeräte GmbH) in the living area (75 m^2, ground level) of a two-story single-family house in Braunschweig (latN: 52° 17′, longE: 10° 27′). The house was built in 1963, was energetically completely refurbished in 2006 in accordance with the specifications of the German Energy Saving Ordinance (EnEV) applicable at that time (U < 0.35 W/(m²·K)) and is manually ventilated. Figure 5 compares experimental data and a simulation with WUFI® Plus, the baseline of the IAQCC building physics model, for the period from July 16, 2020, to August 31, 2020, with a sunny weather period in mid-August. During this period, windows and doors were opened in the morning and evening hours and closed during the day, with the exception of necessary entries and exits. Shading devices were used intensively. A ventilation rate of 0.5 h^{-1} was assumed. Spot ventilation by opening most windows in the morning is accounted for by an increased air exchange of 4 h^{-1} between 08:00 and 09:00. An indoor temperature above 23°C acts as the trigger to activate shading systems on windows, which reduces the passing solar radiation by 60%. In addition, constant shading factors between 0.4 and 0.75 were assumed for the

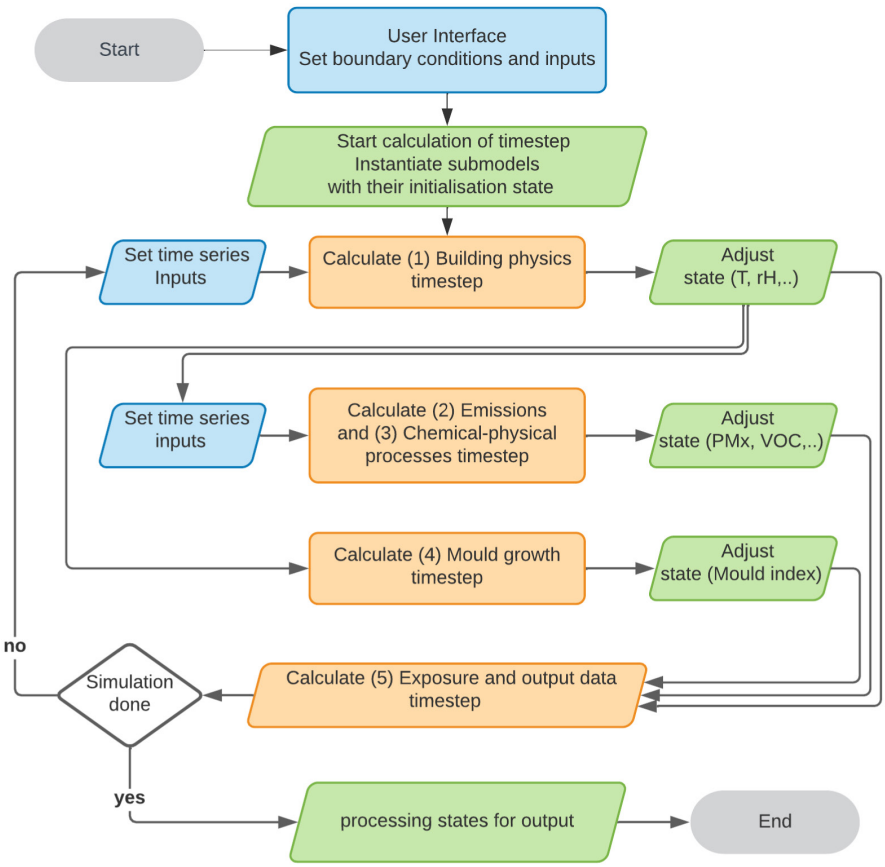

FIGURE 4 Holistic IAQCC model algorithm

south-east and south-west windows. All calculations were made with the WUFI® Plus software.[30] Ambient meteorological parameters driving the building simulation were taken from a nearby state government meteorological station (Air Hygienic Monitoring System Lower Saxony, Station DENI011).

It is noticeable that the calculation predicts the time evolution of indoor temperature (see Figure 5a) and humidity (see Figure 5b) with acceptable accuracy, despite the limited information available on user behavior. This applies both to the course of the day and to the entire period of around six weeks. The data calculated in this way are therefore suitable as input parameters for the emission and exposure models.

In addition, the data can be used to calculate the heat stress index DI (see equation 6) and other indoor comfort indices. The highest outside air temperature measured during the observation period was 34.5°C with a relative humidity of 27.8%. This corresponds to a wet-bulb temperature of 21.2°C and a DI of 30.6, which indicates severe thermal stress. The highest measured indoor air temperature was 26.1°C with a relative humidity of 41.5%. This corresponds to a wet-bulb temperature of 17.6°C and a DI of 25.8, which indicates the onset of thermal stress.

4.2 | Simulation of mold growth

The IAQCC model provides several options to account for the conditions relevant to the growth of mold on surfaces. Dynamic storage, heat, and moisture transport mechanisms in three-dimensional building components determine surface temperature and humidity. This can be considered by dynamically simulating a three-dimensional thermal bridge and computing the resulting surface humidity based on the indoor vapor pressure assuming a well-mixed indoor air. The WUFI® model, which serves as the building component simulation module for the IAQCC model, provides temperature and humidity on one-dimensional building components. A quasi-dynamic method is also added to the IAQCC model system, which uses a temperature factor, the ratio of temperature difference between indoor air temperature to interior surface temperature versus the temperature difference between indoor and outdoor air temperature, to compute the surface temperature on thermal bridges neglecting storage effects.

The same model as described in Section 4.1 is used to demonstrate the capability of the mold model to predict and compare mold growth risk. In contrast to the assumptions above, higher interior loads corresponding to a 5-person family occupying the building were assumed. All other boundary conditions are the same.

Figure 6 shows the results for the mold growth index calculated with the VTT mold model for a simulation period of 6 years. The mold index remains low for well-executed thermal bridges with a temperature factor of 0.9. Thermal bridges with a temperature factor of 0.7, which is the code minimum value in Germany—new buildings or buildings undergoing renovations must show that all thermal bridges exceed this temperature factor, which already leads to a significant mold index above 1.5. A temperature factor of 0.5 would lead to mold growth clearly visible to the human eye reaching a mold index of 3 after less than three years.

4.3 | Emission of gaseous and particulate pollutants

A large amount of data on emission rates of organic compounds and particulate matter is available in the literature. Salthammer[100] offers an overview of construction products, consumer goods, and electronic devices. A comprehensive work on particle sources has been published by Zhao et al.[49] In principle, however, the data for the relevant product and the emitting species must be researched individually in publications and databases.

In addition, temperature-dependent emission rates are only available for a few products.[43,101] The release of formaldehyde from wood-based materials is an exception. Here, the relationship between emission rate, relative humidity, and temperature was examined in detail.[45] For most emission processes, the temperature dependency must be estimated from the available literature. When assuming Arrhenius' law, typical activation energies of organic compounds are in the range between 40 kJ/mol and 120 kJ/mol.[102] Salthammer and Morrison provide an overview of temperature-dependent processes in the indoor environment.[103]

Sink effects can also be very different depending on the substance and the environment.[104,105] With a constant emission rate and no or irreversible sink, the concentration–time profile of an organic compound follows a simple single exponential time law. If, on the contrary, the emission rate is a function of other parameters and the sink is reversible, the kinetics become multi-exponential and thus significantly more complex. The IAQCC emissions module is able to map the common scenarios, for application examples reference is made to the literature.[42,106,107]

For formaldehyde and acetaldehyde, many concentration and emission data have been published. These compounds were selected as non-reactive VVOCs. The same applies to the VOCs n-butyl acetate, n-decane, toluene, acetic acid, and TEP, which cover a wide range of physical properties.

Figure 7 shows a measured outdoor PNSD (a), calculated indoor PNSD when considering only infiltration from ambient air (b), measured indoor PNSD (c), and calculated particle size-resolved source emission rates (d) over 24 hours with one-minute resolution. The experimental data, penetration factor P, and ventilation rate λ were taken from a real scenario reported by Zhao et al.[48] The model takes the measured outdoor PNSD as input and assumes that the initial indoor PNSD is zero. The amount of particles being transported from outside can then be calculated from equation (5).

The loss of indoor particles is caused by exfiltration and particle deposition onto indoor horizontal and vertical surfaces (i.e., ceiling, ground, and walls). The calculation method follows the approach by Lai and Nazaroff.[108] Coagulation loss was estimated for each particle size range by calculating the Brownian coagulation coefficient

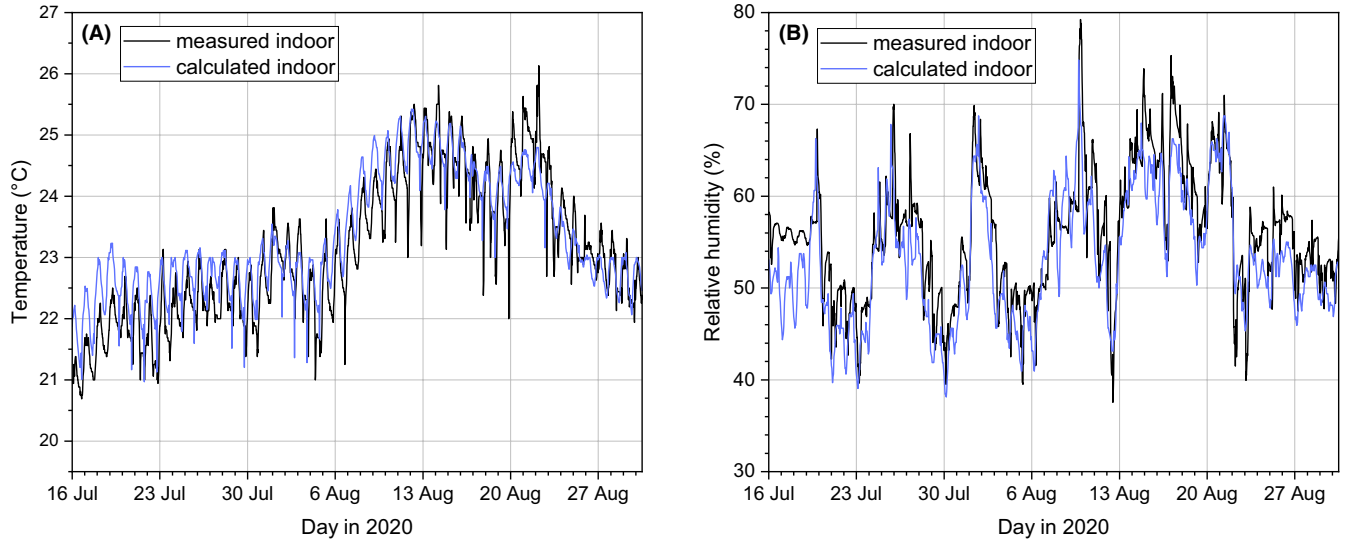

FIGURE 5 Comparison of measured and calculated temperature (a) and humidity (b) for a single-family house in Germany during summer 2020

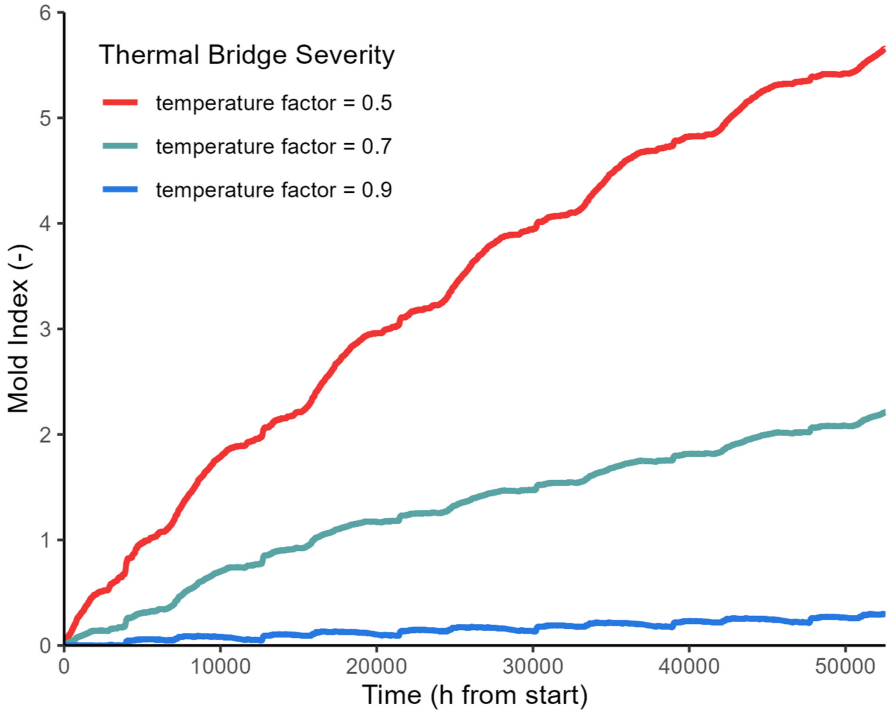

FIGURE 6 Comparison of mold index for thermal bridges with different temperature factors on a single-family house in Germany over the period of six years

between two monodisperse particle populations.[109] The number concentration of new particles formed by coagulation was then redistributed to the two closest size ranges according to the distance ratio of diameters between them. Three indoor particle sources were active around 07:00 (toasting), 14:00 (baking), and 19:00 (cooking) as recorded by residents. The particle size-resolved emission rates (see Figure 7d) could then be extracted by comparing the measured and calculated indoor PNSD. Here, the model was used to calculate emission rates. Correspondingly, particle concentrations can be calculated from known emission rates of these and other sources (printers, combustion, etc.).

4.4 | Indoor chemistry—limonene/ozone/OH example

The reactions of limonene, which occurs in the form of two enantiomers, with ozone and the OH radical are well described in the literature. The bimolecular reaction constants at 298 K are k_{O3} = $21{\cdot}10^{-17}$ $cm^3{\cdot}molecule^{-1}{\cdot}s^{-1}$ and k_{OH} = $164{\cdot}10^{-12}$ $cm^3{\cdot}molecule^{-1}{\cdot}s^{-1}$, respectively.[110] In addition, both reactions follow Arrhenius' law according to equations (7) and (8).[110]

$$k_{O3}(T) = 2.95 \bullet 10^{-15}(cm^3 \bullet molecule^{-1} \bullet s^{-1}) \bullet e^{-\frac{783K}{T}} \quad (7)$$

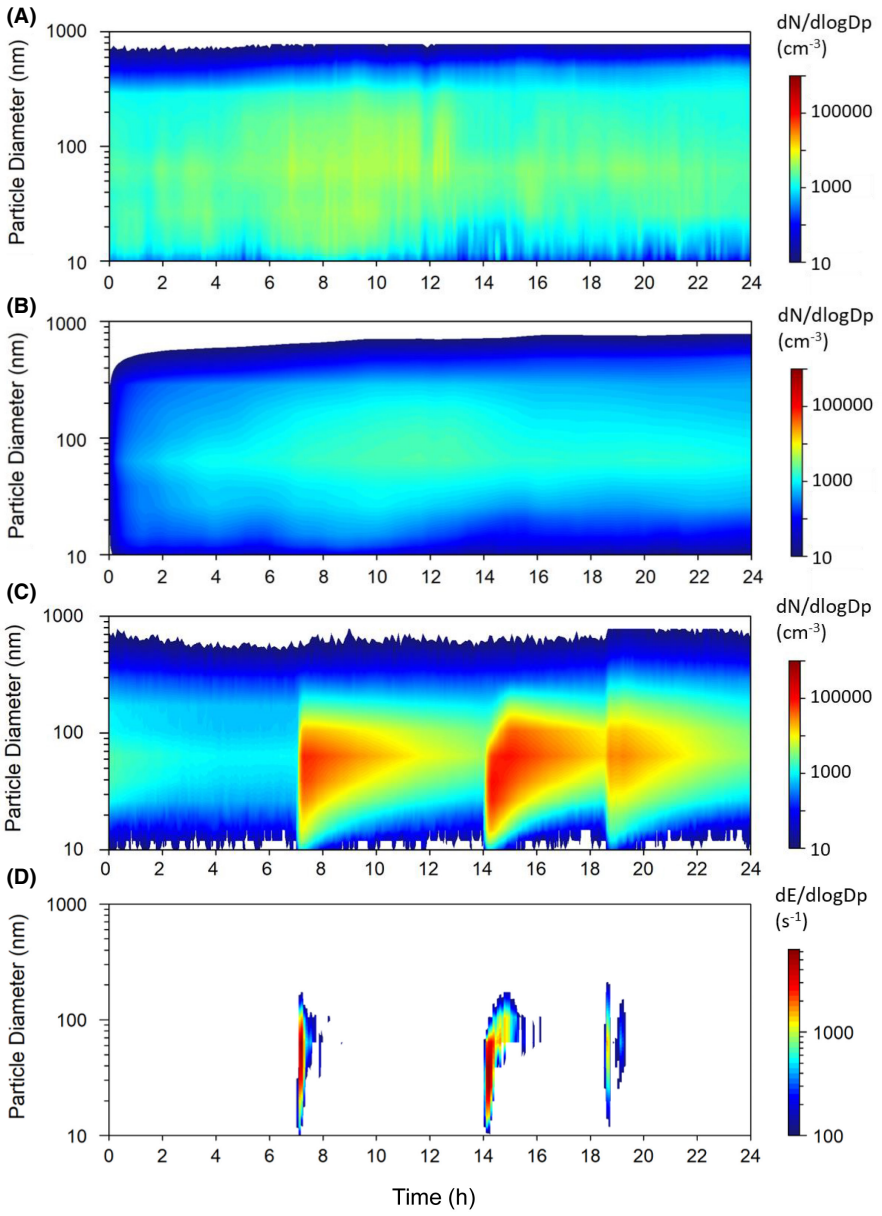

FIGURE 7 a) measured outdoor PNSD; b) calculated non-source indoor PNSD based on outdoor PNSD; c) measured total indoor PNSD with influence of indoor sources; d) calculated size-resolved particle number emission rate of three indoor sources (toasting, baking, and cooking).[48]

$$k_{OH}(T) = 4.28 \bullet 10^{-11}(cm^3 \bullet molecule^{-1} \bullet s^{-1}) \bullet e^{\frac{401K}{T}} \quad (8)$$

A 24-hour scenario was chosen for this demonstrative simulation (see Figure 8). A constantly emitting air freshener was assumed as limonene source with an emission rate of SER_u = 6000 µg/h at 298 K in a 50 m³ room. The release was evaporation-controlled and thus only depended on the vaporization enthalpy $\Delta_{vap}H$ = 49.6 kJ/mol of limonene.[111] The temperature dependence of SER_u could then be determined using equation (9), which was derived from the Clausius-Clapeyron equation.

$$\ln SER_{u(T_2)} = \ln SER_{u(T_1)} - \frac{\Delta_{vap}H}{R}\left(\frac{1}{T_2} - \frac{1}{T_1}\right) \quad (9)$$

Outdoor temperature, relative humidity, and ozone concentration data were taken from the state government monitoring station Braunschweig (DENI011) for August 14, 2020. Indoor temperature and relative humidity were calculated as described in Section 4.1. A typical summertime ventilation pattern for Germany was applied: during nighttime hours (23:00–08:00) windows tilted (λ = 1.5 h^{-1}); during daytime hours (08:00–19:00) windows closed (λ = 0.5 h^{-1}); and during evening hours (19:00–23:00) windows wide open (λ = 3.0 h^{-1}).[4] The diurnal time series of outdoor OH radical concentration was taken from a measurement during summer time near London,[112] where the concentration ranged from $1{\cdot}10^{-5}$ ppb to $1{\cdot}10^{-4}$ ppb ($2.5{\cdot}10^5$–$2.5{\cdot}10^6$ molecules·cm^{-3}). This can be considered typical for a summer day in Central Europe.[113] The indoor deposition velocities for ozone of 0.036 cm/s and the OH radical of 0.07 cm/s were taken from the literature.[114]

Figure 8a–d includes the 24 h concentration curves for the full scenario with a temporal resolution of 1 min. Temperature and humidity data are shown in Figure 8a. The air exchange rates assumed for certain day and night times are shown in Figure 8b together with

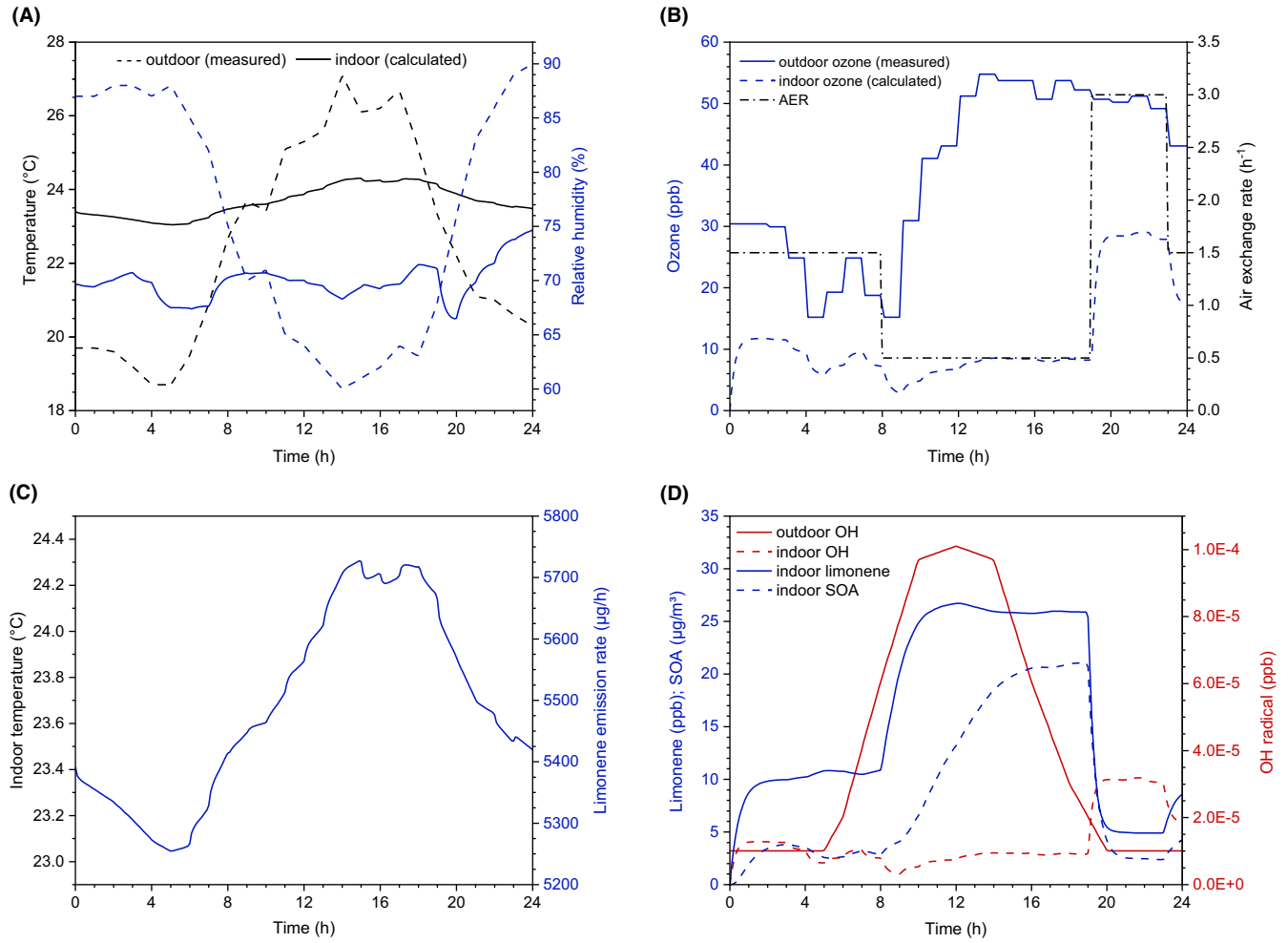

FIGURE 8 a) Outdoor temperature and relative humidity measured on August 14, 2020 in Braunschweig, Germany, and indoor air values calculated with the scenario discussed in Section 4.1. b) Outdoor air ozone concentrations for August 14, 2020 in the area of Braunschweig, Germany, and calculated indoor air ozone concentrations. The scenario described by Salthammer et al.[4] was used for the air exchange rates. c) Temperature dependence of the limonene source emission rate calculated according to equation (9) with $SER_u(298\ K) = 6000\ \mu g/h$ and $\Delta_{vap}H = 49.6$ kJ/mol. Note that the limonene curve also represents the temperature. d) OH radical concentrations measured outdoors[112] and calculated indoors, calculated limonene concentrations assuming a room volume of 50 m³, and calculated SOA concentration from the limonene/ozone reaction with $\xi = 0.5$

the ozone data for outdoor air and indoor air. The limonene emission rate in dependence of temperature and time is shown in Figure 8c. Finally, Figure 8d shows the concentration profiles for the indoor and outdoor OH radical, limonene and produced SOA.

The concentration of ozone in the room air during nighttime and daytime was around 10 ppb (19.6 µg/m³ at p = 1013 hPa and T = 298 K). Taking into account ozone outside air concentrations in summer,[4] loss due to ventilation, and typical degradation rates indoors,[115] this was at the lower end. OH production from limonene and ozone was also taken into account with an OH yield of 0.86.[114] Indoor OH radical concentrations were estimated based on the work of Weschler and Shields,[116] assuming that OH concentrations reach an equilibrium state at each simulation time interval, where sinks include ventilation, deposition, and reaction with limonene, and sources include outdoor air contribution and limonene/ozone reaction. The simulated indoor OH concentrations were in a range expected for an indoor space with terpene sources.[117] Due to the limited number of target compounds, the contribution of other reaction pathways, for example, inorganics and HONO, was not considered here.

The removal rate of limonene by ozone at 10 ppb and 30 ppb was ≈0.2 h^{-1} and ≈0.6 h^{-1}, respectively. The major product in the initial gas-phase ozonolysis of limonene was the secondary endo-ozonide $C_{10}H_{16}O_3$.[118] The produced OH radicals also consumed limonene, with removal rates of ≈0.1 h^{-1} and ≈0.4 h^{-1} for OH concentrations of $1{\cdot}10^{-5}$ ppb and $3{\cdot}10^{-5}$ ppb, respectively. In the morning, the indoor limonene concentration increases from ≈10 ppb to ≈25 ppb (139.3 µg/m³ at p = 1013 hPa and T = 298 K), which can be attributed to the decreased ventilation rate λ (from 1.5 h^{-1} to 0.5 h^{-1} at 08:00) and the increasing emission rate of the air freshener due to the rising temperature. Between 19:00 and 23:00, the loss of limonene was mainly due to the high air exchange rate of $\lambda = 3\ h^{-1}$, which leads to an increase in ozone and OH during this period.

The concentration versus time curve for SOA in Figure 8d must be taken as a rough estimate. It is only intended to show the magnitude of the generated particle mass. A value of $\xi = 0.5$ was chosen as the SOA yield for the limonene/ozone system. This is essentially based on the work of Saathoff et al.,[74] who measured SOA yields between 0.47 and 0.76 for the limonene/ozone system at 293 K, limonene concentrations of 77–262 µg/m³, and background aerosol concentrations of 28–477 µg/m³. Coleman et al.[119] indicate SOA yields of up to 0.37 for the reaction of terpene-rich household products with ozone. The maximum SOA values calculated under the conditions of this work are in the range of 20 µg/m³. This corresponds approximately to the values specified by Waring[77] for 10 ppb ozone, 25 ppb limonene, and an air change rate of 0.5 h^{-1}.

For isoprene (2-methyl-1,3-butadiene), the other reactive species selected as a model compound, the reaction constants at 298 K are $k_{O3} = 1.27{\cdot}10^{-17}$ cm³·molecule^{-1}·s^{-1} and $k_{OH} = 100{\cdot}10^{-12}$ cm³·molecule^{-1}·s^{-1}. Arrhenius parameters are also available.[110]

In later versions of the model, competitive reactions via nitrate radicals may also have to be taken into account. The bimolecular reaction constant to limonene at 298 K is $k_{NO3} = 1.22{\cdot}10^{-11}$ cm³·molecule^{-1}·s^{-1}.[110] For typical concentrations of 20 ppb ozone, $6.7{\cdot}10^{-6}$ ppb OH[116] and 0.001 ppb NO_3[120] the respective limonene lifetimes τ are 2.7 h, 10.3 h and 0.9 h with $\tau = 1/(k{\cdot}[\text{reactant}])$. The lifetime of a substance with respect to a given reactant is the decrease to 1/e of the initial concentration.

4.5 | Gas/particle distribution of SVOCs

Benzophenone, TXIB, and DEHA were chosen as SVOCs because of their different distribution coefficients. Simulating SVOC concentrations in indoor air is more difficult than for VOCs because not only sinks but also gas/particle equilibria must be considered. For the IAQCC model, the approach by Finizio et al.,[83] which is based on the K_{OA} value and the organic particle fraction f_{om_part} according to equation (10), is used to calculate the gas/particle coefficient K_p of an SVOC. According to Bidleman and Harner,[121] $f_{om\_part} = 0.2$ by default.

$$\log K_p = \log K_{OA} + \log f_{om\_part} - 11.91 \quad (10)$$

The fraction Φ of the respective SVOC is then calculated from equation (4). Figure 9 shows Φ as a function of log K_{OA}. It can be seen that even with a high total particle concentration of [TSP] = 100 µg/m³ more than 10% of the SVOC is sorbed in the particle phase from a log K_{OA} of 9.6. However, due to the roughly estimated value of f_{om_part}, Φ is subject to greater uncertainties.

Since distribution coefficients are temperature dependent, the IAQCC model may need to make adjustments for the respective climatic conditions. Usually, values for 298 K are available. Factors and enthalpies for conversion to other temperatures have been published for various substances.[29,122,123]

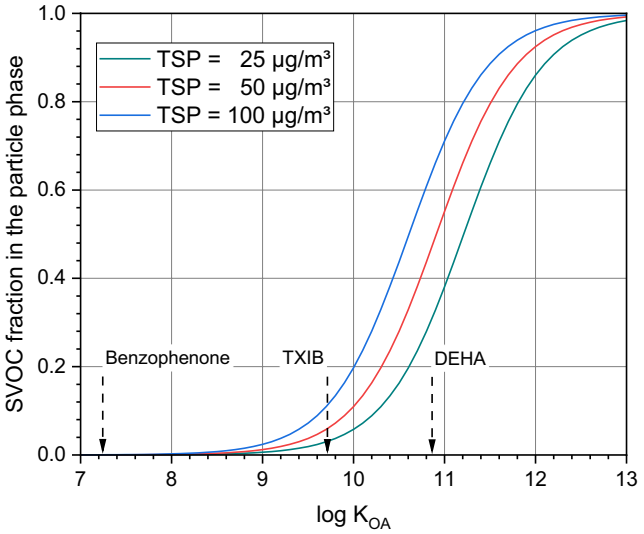

FIGURE 9 Fraction of an SVOC in the particle phase as a function of log K_{OA} at different total suspended particle concentrations (TSP). It was assumed that the particles consist of 20% organic material ($f_{om\_part} = 0.2$)

Liu et al. (2013)[124] pointed out that the assumption of instantaneous gas/particle equilibrium can lead to large errors in the estimation of indoor SVOC concentrations. Therefore, in this work, the estimation of SVOC concentration is treated as a post-processing module, that is, first the indoor TSP is quantified and then the sorbed SVOC on the particles is estimated using Equation (3) for a longer time period. The TSP is assumed to be indoor PM_{10}. According to the work of Weschler and Nazaroff,[125] the time scale to achieve equilibrium sorption (τ) for our target SVOCs ranges from 1 h to 1 day.

5 | FINALIZATION OF THE MODEL—FURTHER WORK

With the indoor air quality climate change (IAQCC), a holistic approach is presented that combines climatic and chemical–physical models. In this work, it was shown that the temporal variation of temperature and humidity in a living space can be simulated accurately over a long-term period, assuming a simple building setup and activity parameters. The ambient air data required for this can be obtained from the dense European measurement station network. In addition, many measuring stations provide hourly data for ozone and particle concentrations. This allows realistic calculations for the entry of ozone and particulate matter (PM) into the indoor environment.

A key feature of IAQCC is the long-term forecast of the indoor climate to be expected in the future based on the assumptions and scenarios provided by the International Panel on Climate Change (IPCC). The IAQCC model also allows an assessment of the future risk of indoor mold growth, as higher peak temperature, higher humidity, and overall greater temperature fluctuations are expected in

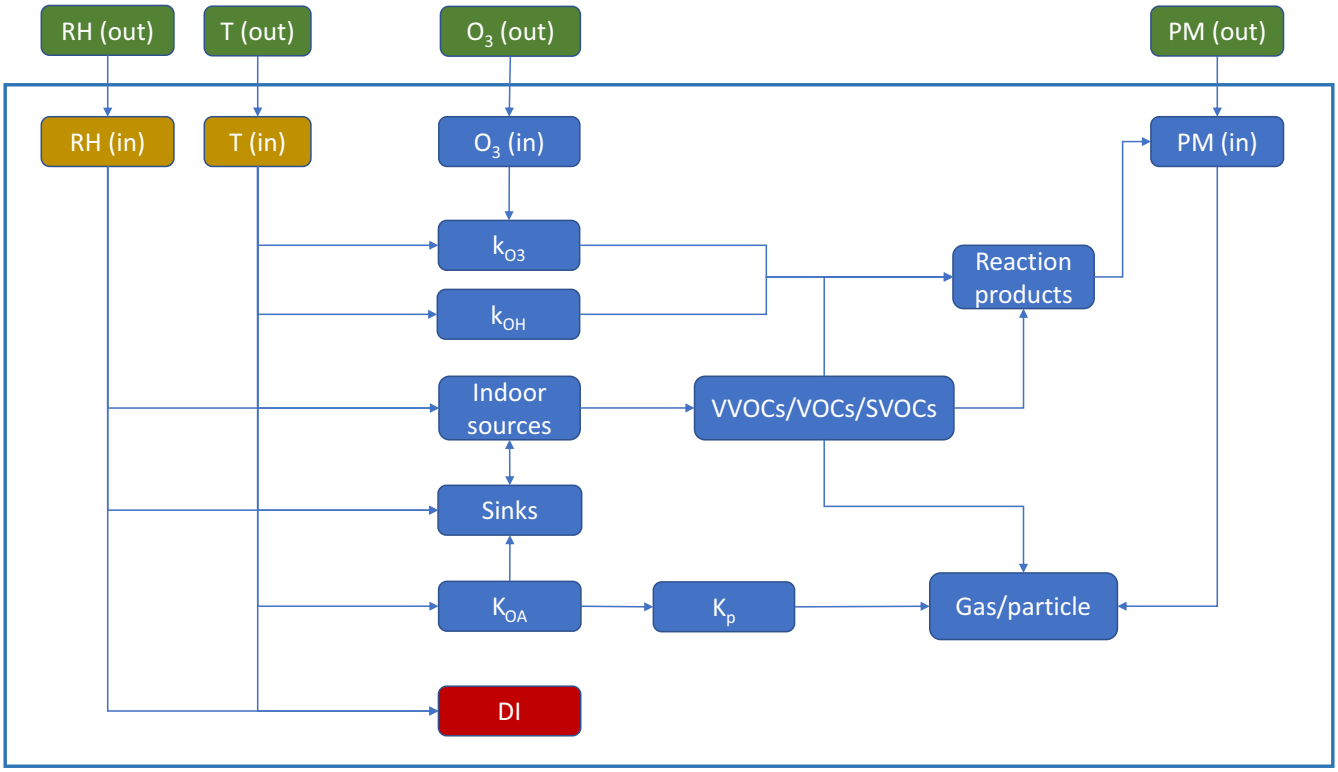

FIGURE 10 Overview of the relationships between climatic parameters, emissions, chemical reactions and interaction of indoor pollutants taken into account by the IAQCC model

the future. IAQCC can also be used to assess possible changes in indoor pollutant concentrations for given scenarios that prescribe building properties, state of ventilation, occupant lifestyle, and anticipated changes in ambient pollutant concentrations.

Partition coefficients and rate constants for the reaction with ozone and OH radicals are well known for many substances. This also applies to temperature dependencies. However, only gas-phase reactions are included in IAQCC. Surface reactions to materials or on the skin are not implemented. Such a detailed treatment is not the task of the model. Moreover, the very complex kinetics of dermal sorption,[126] which would also have to take into account the influence of clothing and its ingredients,[127] remains unconsidered. Our modeled air concentrations should preferably be evaluated using guide values. These are usually based on inhalation.

Material-specific emission rates and typical indoor concentrations are available for many substances at room temperature. Temperature-dependent data are only published sporadically. In order to be as realistic as possible estimates have to be used in the IAQCC, for example Arrhenius relationships. Assumptions also have to be made to consider sink effects, as these vary greatly depending on the substance and the environment. For model development and testing, only the 12 substances shown in Table 1 are initially taken into account. The model is conceived so that further substances can be implemented.

As can be seen from Figure 10, there are complex relationships between the individual submodels, although these are only shown here in a simplified manner. In the next step, the chemical–physical parameters necessary for the technical realization of the model are evaluated and linked on the basis of the routines presented here. With this, short-term and long-term calculations for indoor exposure are made. Consequently, further work will deal with the results of the full approach as shown in Figure 1.

It is undisputed that the immediate effects of climate change such as heat stress, droughts, and extreme weather events are the major problem globally. Nevertheless, it is surprising that the associated influence on indoor climate and indoor air quality has received rather little attention. The IAQCC model was developed as a versatile tool to cover this widely neglected aspect and make predictions that can support decision-making for preventive measures in the frame of building construction, ventilation, and lifestyle.

AUTHOR CONTRIBUTION

Tunga Salthammer: Conceptualization; Funding acquisition; Project administration; Investigation; Visualization; Writing–original draft preparation. Jiangyue Zhao: Investigation; Methodology; Visualization; Writing–original draft preparation. Alexandra Schieweck: Funding acquisition; Project administration; Writing–review & editing. Erik Uhde: Methodology; Validation; Writing–review & editing. Tareq Hussein: Investigation; Methodology; Writing–review & editing. Florian Antretter: Investigation; Methodology; Writing–review & editing. Hartwig Künzel: Investigation; Methodology; Validation; Funding acquisition. Matthias Pazold: Investigation; Visualization; Writing–review

& editing. Jan Radon Investigation; Methodology; Writing–review & editing. Wolfram Birmili: Conceptualization; Funding acquisition; Writing–review & editing.

ACKNOWLEDGMENTS

This work was supported by the Federal Ministry for the Environment, Nature Conservation, and Nuclear Safety (BMU) grant REFOPLAN FKZ 3719 51 205 0 (title translated from German: "Influence of climate change on indoor air quality: expert system, quantitative projections, and information system for the public"). Tareq Hussein is grateful for financial support from a Fraunhofer WKI Fellowship. All authors thank the members of the advisory board: Professor Nicola Carslaw, Professor Dusan Licina, Professor Andreas Holm, Dr. Ana Maria Scutaru, and Mrs. Anja Daniels.

CONFLICT OF INTEREST

The authors declare that they have no competing financial interests or personal relationships that could have appeared to influence the work reported in this paper.

PEER REVIEW

The peer review history for this article is available at https://publons.com/publon/10.1111/ina.13039.

ORCID

Tunga Salthammer https://orcid.org/0000-0002-2370-8664
Jiangyue Zhao https://orcid.org/0000-0001-5202-239X
Alexandra Schieweck https://orcid.org/0000-0003-2523-9934
Erik Uhde https://orcid.org/0000-0002-8704-3702
Tareq Hussein https://orcid.org/0000-0002-0241-6435
Florian Antretter https://orcid.org/0000-0002-9725-1257
Hartwig Künzel https://orcid.org/0000-0001-8305-0262
Jan Radon https://orcid.org/0000-0002-2119-4903
Wolfram Birmili https://orcid.org/0000-0002-5295-6333

REFERENCES

1. IPCC. *Climate Change 2021: The Physical Science Basis*. Cambridge University Press; 2021.
2. Brasseur GP, Jacob D, Schuck-Zöller S, eds. *Klimawandel in Deutschland*. Springer Spektrum; 2017.
3. Baklanov A, Molina LT, Gauss M. Megacities, air quality and climate. *Atmos Environ*. 2016;126:235-249.
4. Salthammer T, Schieweck A, Gu J, Ameri S, Uhde E. Future trends in ambient air pollution and climate in Germany – Implications for the indoor environment. *Build Environ*. 2018;143:661-670.
5. Leech JA, Nelson WC, Burnett RT, Aaron S, Raizenne ME. It's about time: A comparison of Canadian and American time-activity patterns. *J Expo Anal Environ Epidemiol*. 2002;12:427-432.
6. Brasche S, Bischof W. Daily time spent indoors in German homes - baseline data for the assessment of indoor exposure of German occupants. *Int J Hyg Environ Health*. 2005;208:247-253.
7. Nazaroff WW. Exploring the consequences of climate change for indoor air quality. *Environ Res Lett*. 2013;8: 015022.
8. Spengler JD. Climate change, indoor environments, and health. *Indoor Air*. 2012;22:89-95.
9. Fisk WJ. Review of some effects of climate change on indoor environmental quality and health and associated no-regrets mitigation measures. *Build Environ*. 2015;86:70-80.
10. IOM - Institute of Medicine. *Climate Change, the Indoor Environment, and Health*. The National Academies Press; 2011.
11. Jacobson MZ. *Air Pollution and Global Warming*. Cambridge University Press; 2012.
12. Papanastasiou DK, Melas D, Kambezidis HD. Air quality and thermal comfort levels under extreme hot weather. *Atmos Res*. 2015;152:4-13.
13. Lindemann U, Stotz A, Beyer N, et al. Effect of indoor temperature on physical performance in older adults during days with normal temperature and heat waves. *Int J Environ Res Public Health*. 2017;14:186.
14. Hamdy M, Carlucci S, Hoes P-J, Hensen JLM. The impact of climate change on the overheating risk in dwellings—A Dutch case study. *Build Environ*. 2017;122(Supplement C):307–323.
15. O'Lenick CR, Wilhelmi OV, Michael R, et al. Urban heat and air pollution: A framework for integrating population vulnerability and indoor exposure in health risk analyses. *Sci Total Environ*. 2019;660:715-723.
16. Tham S, Thompson R, Landeg O, Murray KA, Waite T. Indoor temperature and health: a global systematic review. *Public Health*. 2020;179:9-17.
17. Fischer PH, Brunekreef B, Lebret E. Air pollution related deaths during the 2003 heat wave in the Netherlands. *Atmos Environ*. 2004;38:1083-1085.
18. Barriopedro D, Fischer EM, Luterbacher J, Trigo RM, García-Herrera R. The hot summer of 2010: Redrawing the temperature record map of Europe. *Science*. 2011;332:220-224.
19. Steul K, Schade M, Heudorf U. Mortality during heatwaves 2003–2015 in Frankfurt-Main – the 2003 heatwave and its implications. *Int J Hyg Environ Health*. 2018;221:81-86.
20. Lee J, Lewis A, Monks P, et al. Ozone photochemistry and elevated isoprene during the UK heatwave of august 2003. *Atmos Environ*. 2006;40:7598-7613.
21. Asumadu-Sakyi AB, Barnett AG, Thai P, et al. The relationship between indoor and outdoor temperature in warm and cool seasons in houses in Brisbane, Australia. *Energy Buildings*. 2019;191:127-142.
22. Asumadu-Sakyi AB, Miller W, Barnett AG, et al. Seasonal temperature patterns and durations of acceptable temperature range in houses in Brisbane, Australia. *Sci Total Environ*. 2019;683:470-479.
23. Lundgren Kownacki K, Gao C, Kuklane K, Wierzbicka A. Heat stress in indoor environments of Scandinavian urban areas: A literature review. *Int J Environ Res Public Health*. 2019;16:560.
24. Künzel HM. Verfahren zur ein-und zweidimensionalen Berechnung des gekoppelten Wärme-und Feuchtetransports in Bauteilen mit einfachen Kennwerten. Dissertation; Stuttgart; 1994.
25. Shiraiwa M, Carslaw N, Tobias DJ, et al. Modelling consortium for chemistry of indoor environments (MOCCIE): integrating chemical processes from molecular to room scales. *Environ Sci: Processes & Impacts*. 2019;21:1240-1254.
26. Štejfa V, Fulem M, Růžička K, Morávek P. New static apparatus for vapor pressure measurements: Reconciled thermophysical data for benzophenone. *J Chem Eng Data*. 2016;61:3627-3639.
27. Salthammer T, Grimme S, Stahn M, Hohm U, Palm W-U. Quantum chemical calculation and evaluation of partition coefficients for classical and emerging environmentally relevant organic compounds. *Environ Sci Technol*. 2021;56:379-391.
28. Sander R. Compilation of Henry's law constants (version 4.0) for water as solvent. *Atmos Chem Phys*. 2015;15(8):4399-4981.
29. Baskaran S, Lei YD, Wania F. A Database of experimentally derived and estimated octanol–air partition ratios (K_{OA}). *J Phys Chem Ref Data*. 2021;50: 043101.

30. Antretter F, Sauer F, Schöpfer T, Holm A. Validation of a hygrothermal whole building simulation software. Proceedings of Building Simulation 2011: 12th Conference of International Building Performance Simulation Association. Sydney; 2011:1694–1701.
31. Schmidt E. *Properties of Water and Steam in SI-Units*. Springer Verlag; 1979.
32. Antretter F, Pazold M, Radon J, Künzel H. Kopplung von dynamischer Wärmebrückenberechnung mit hygrothermischer Gebäudesimulation. *Bauphysik*. 2013;35:181-192.
33. Pazold M, Antretter F. Hygrothermische Gebäudesimulation mit Multizonen-Gebäudedurchströmungsmodell. *Bauphysik*. 2013;35:86-92.
34. Little JC, Hodgson AT, Gadgil AJ. Modeling emissions of volatile organic compounds from new carpets. *Atmos Environ*. 1994;28:227-234.
35. Cox SS, Little JC, Hodgson AT. Predicting the emission rate of volatile organic compounds from vinyl flooring. *Environ Sci Technol*. 2002;36:709-714.
36. Tichenor BA, Guo Z, Sparks LE. Fundamental mass transfer model for indoor air emissions from surface coatings. *Indoor Air*. 1993;3:263-268.
37. Liu Z, Ye W, Little JC. Predicting emissions of volatile and semivolatile organic compounds from building materials: A review. *Build Environ*. 2013;64:7-25.
38. Wei W, Mandin C, Ramalho O. Influence of indoor environmental factors on mass transfer parameters and concentrations of semivolatile organic compounds. *Chemosphere*. 2018;195:223-235.
39. Xiong J, Chen F, Sun L, et al. Characterization of VOC emissions from composite wood furniture: Parameter determination and simplified model. *Build Environ*. 2019;161:106237.
40. Salthammer T. Calculation of kinetic parameters from chamber tests using nonlinear regression. *Atmos Environ*. 1996;30:161-171.
41. Colombo A, De Bortoli M, Pecchio E, Schauenburg H, Schlitt H, Vissers H. Chamber testing of organic emission from building and furnishing materials. *Sci Total Environ*. 1990;91:237-249.
42. Dunn JE, Tichenor BA. Compensating for sink effects in emission test chambers by mathematical modeling. *Atmos Environ*. 1988;22:885-894.
43. Xiong J, Wei W, Huang S, Zhang Y. Association between the emission rate and temperature for chemical pollutants in building materials: General correlation and understanding. *Environ Sci Technol*. 2013;47:8540-8547.
44. Liang Y, Xu Y. Emission of phthalates and phthalate alternatives from vinyl flooring and crib mattress covers: The Influence of Temperature. *Environ Sci Technol*. 2014;48:14228-14237.
45. Meyer B, Greubel D, Schwab H, Marutzky R. Formaldehydemissionen aus Spanplatten Aktualisierung des WKI-Rechenmodells. *Holztechnologie*. 2014;55:20-26.
46. Bope A, Haines SR, Hegarty B, Weschler CJ, Peccia J, Dannemiller KC. Degradation of phthalate esters in floor dust at elevated relative humidity. *Environ Sci Processes Impacts*. 2019;21:1268-1279.
47. Zhao J, Weinhold K, Merkel M, et al. Concept of high quality simultaneous measurements of the indoor and outdoor aerosol to determine the exposure to fine and ultrafine particles in private homes. *Gefahrstoffe Reinhalt Luft*. 2018;78:73-78.
48. Zhao J, Birmili W, Wehner B, et al. Particle mass concentrations and number size distributions in 40 homes in germany: Indoor-to-outdoor relationships, diurnal and seasonal variation. *Aerosol Air Qual. Res*. 2020;20:576-589.
49. Zhao J, Birmili W, Hussein T, Wehner B, Wiedensohler A. Particle number emission rates of aerosol sources in 40 German households and their contributions to ultrafine and fine particle exposure. *Indoor Air*. 2021;31:818-831.
50. Salthammer T, Schripp T, Wientzek S, Wensing M. Impact of operating wood-burning fireplace ovens on indoor air quality. *Chemosphere*. 2014;103:205-211.
51. Schripp T, Salthammer T, Wientzek S, Wensing M. chamber studies on nonvented decorative fireplaces using liquid or gelled ethanol fuel. *Environ Sci Technol*. 2014;48:3583-3590.
52. Salthammer T, Gu J, Wientzek S, Harrington R, Thomann S. Measurement and evaluation of gaseous and particulate emissions from burning scented and unscented candles. *Environ Int*. 2021;155:106590.
53. Klosterköther A, Kurtenbach R, Wiesen P, Kleffmann J. Determination of the emission indices for NO, NO2, HONO, HCHO, CO, and particles emitted from candles. *Indoor Air*. 2020;31:116-127.
54. Stabile L, Fuoco FC, Buonanno G. Characteristics of particles and black carbon emitted by combustion of incenses, candles and anti-mosquito products. *Build Environ*. 2012;56:184-191.
55. Buonanno G, Morawska L, Stabile L. Particle emission factors during cooking activities. *Atmos Environ*. 2009;43:3235-3242.
56. Jørgensen RB, Strandberg B, Sjaastad AK, Johansen A, Svendsen K. Simulated restaurant cook exposure to emissions of PAHs, mutagenic aldehydes, and particles from frying bacon. *J Occup Environ Hyg*. 2013;10:122-131.
57. Gu J, Uhde E, Wensing M, Xia F, Salthammer T. emission control of desktop 3D printing: The effects of a filter cover and an air purifier. *Environ Sci Technol Letters*. 2019;6(8):499-503.
58. Gu J, Karrasch S, Salthammer T. Review of the characteristics and possible health effects of particles emitted from laser printing devices. *Indoor Air*. 2020;30:396-421.
59. Pirela SV, Martin J, Bello D, Demokritou P. Nanoparticle exposures from nano-enabled toner-based printing equipment and human health: state of science and future research needs. *Crit Rev Toxicol*. 2017;47:678-704.
60. Azimi P, Zhao D, Pouzet C, Crain NE, Stephens B. Emissions of ultrafine particles and volatile organic compounds from commercially available desktop three-dimensional printers with multiple filaments. *Environ Sci Technol*. 2016;50:1260-1268.
61. Bekö G, Weschler CJ, Wierzbicka A, et al. ultrafine particles: exposure and source apportionment in 56 Danish homes. *Environ Sci Technol*. 2013;47:10240-10248.
62. Isaxon C, Gudmundsson A, Nordin EZ, et al. Contribution of indoor-generated particles to residential exposure. *Atmos Environ*. 2015;106:458-466.
63. Géhin E, Ramalho O, Kirchner S. Size distribution and emission rate measurement of fine and ultrafine particle from indoor human activities. *Atmos Environ*. 2008;42:8341-8352.
64. Glytsos T, Ondrácek J, Dzumbová L, Kopanakis I, Lazaridis M. Characterization of particulate matter concentrations during controlled indoor activities. *Atmos Environ*. 2010;44:1539-1549.
65. Hussein T, Glytsos T, Ondráček J, et al. Particle size characterization and emission rates during indoor activities in a house. *Atmos Environ*. 2006;40:4285-4307.
66. Dimitroulopoulou C, Lucica E, Johnson A, et al. EPHECT I: European household survey on domestic use of consumer products and development of worst-case scenarios for daily use. *Sci Total Environ*. 2015;536:880-889.
67. Dimitroulopoulou C, Trantallidi M, Carrer P, Efthimiou GC, Bartzis JG. EPHECT II: Exposure assessment to household consumer products. *Sci Total Environ*. 2015;536:890-902.
68. Trantallidi M, Dimitroulopoulou C, Wolkoff P, Kephalopoulos S, Carrer P. EPHECT III: Health risk assessment of exposure to household consumer products. *Sci Total Environ*. 2015;536:903-913.
69. Hussein T, Korhonen H, Herrmann E, Hämeri K, Lehtinen KEJ, Kulmala M. Emission rates due to indoor activities: Indoor aerosol model development, evaluation, and applications. *Aerosol Sci Technol*. 2005;39:1111-1127.
70. Hussein T, Kulmala M. Indoor aerosol modeling: Basic principles and practical applications. *Water Air Soil Pollut Focus*. 2008;8:23-34.

71. Hussein T, Wierzbicka A, Löndahl J, Lazaridis M, Hänninen O. Indoor aerosol modeling for assessment of exposure and respiratory tract deposited dose. *Atmos Environ*. 2015;106:402-411.
72. Jenkin ME, Saunders SM, Pilling MJ. The tropospheric degradation of volatile organic compounds: A protocol for mechanism development. *Atmos Environ*. 1997;31:81-104.
73. Odum JR, Hoffmann T, Bowman F, Collins D, Flagan RC, Seinfeld JH. Gas/particle partitioning and secondary organic aerosol yields. *Environ Sci Technol*. 1996;30:2580-2585.
74. Saathoff H, Naumann KH, Möhler O, et al. Temperature dependence of yields of secondary organic aerosols from the ozonolysis of a-pinene and limonene. *Atmos Chem Phys*. 2009;9:1551-1577.
75. Leungsakul S, Jaoui M, Kamens RM. Kinetic mechanism for predicting secondary organic aerosol formation from the reaction of d-limonene with ozone. *Environ Sci Technol*. 2005;39:9583-9594.
76. Waring MS. Secondary organic aerosol in residences: Predicting its fraction of fine particle mass and determinants of formation strength. *Indoor Air*. 2014;24:376-389.
77. Waring MS. Secondary organic aerosol formation by limonene ozonolysis: Parameterizing multi-generational chemistry in ozone- and residence time-limited indoor environments. *Atmos Environ*. 2016;144:79-86.
78. Youssefi S, Waring MS. Predicting secondary organic aerosol formation from terpenoid ozonolysis with varying yields in indoor environments. *Indoor Air*. 2012;22(5):415-426.
79. Salthammer T, Zhang Y, Mo J, Koch HM, Weschler CJ. Assessing human exposure to organic pollutants in the indoor environment. *Angew Chem Int Ed*. 2018;57:12228-12263.
80. Eichler CMA, Hubal EAC, Xu Y, et al. Assessing human exposure to SVOCs in materials, products, and articles: A modular mechanistic framework. *Environ Sci Technol*. 2020;55:25-43.
81. Pankow JF. Review and comparative analysis of the theories on partitioning between the gas and aerosol particulate phases in the atmosphere. *Atmos Environ*. 1987;21:2275-2283.
82. Pankow JF. An absorption model of the gas/aerosol partitioning involved in the formation of secondary organic aerosol. *Atmos Environ*. 1994;28:189-193.
83. Finizio A, Mackay D, Bidleman T, Harner T. Octanol-air partition coefficient as a predictor of partitioning of semi-volatile organic chemicals to aerosols. *Atmos Environ*. 1997;31:2289-2296.
84. Vereecken E, Roels S. Review of mould prediction models and their influence on mould risk evaluation. *Build Environ*. 2012;51:296-310.
85. Vereecken E, Vanoirbeek K, Roels S. Towards a more thoughtful use of mould prediction models: A critical view on experimental mould growth research. *J Building Phys*. 2015;39:102-123.
86. Sedlbauer K. Vorhersage von Schimmelpilzbildung auf und in Bauteilen. Dissertation; Stuttgart; 2001.
87. Hukka A, Viitanen HA. A mathematical model of mould growth on wooden material. *Wood Sci Technol*. 1999;33:475-485.
88. Viitanen H, Ojanen T. Improved model to predict mold growth in building materials. Proceedings of the 10th Thermal Performance of the Exterior Envelopes of Whole Buildings Conference. Atlanta; 2007
89. Glass SV, Gatland SD, Ueno K, Schumacher CJ. Analysis of Improved Criteria for Mold Growth in ASHRAE Standard 160 by Comparison with Field Observations. In: Mukhopadhyaya P, Fisler D, eds. *Advances in Hygrothermal Performance of Building Envelopes: Materials, Systems and Simulations*. ASTM International; 2017:1-27.
90. ASHRAE. *Criteria for moisture-control design analysis in buildings - Standard 160P*. ASHRAE; 2016.
91. Viitanen H, Krus M, Ojanen T, Eitner V, Zirkelbach D. Mold risk classification based on comparative evaluation of two established growth models. *Energy Procedia*. 2015;78:1425-1430.
92. Thom EC. The discomfort index. *Weatherwise*. 1959;12:57-61.
93. Epstein Y, Moran DS. Thermal comfort and the heat stress indices. *Ind Health*. 2006;44:388-398.
94. Stull R. Wet-Bulb temperature from relative humidity and air temperature. *J Appl Meteorol Climatol*. 2011;50:2267-2269.
95. ISO 7243. *Ergonomics of the thermal environment — Assessment of heat stress using the WBGT (wet bulb globe temperature) index*. Beuth Verlag; 2017.
96. McArdle WD, Katch FI, Katch VL. *Exercise Physiology: Nutrition, Energy, and Human Performance*. Wolters Kluwer; 2014.
97. Hussein T, Löndahl J, Paasonen P, et al. Modeling regional deposited dose of submicron aerosol particles. *Sci Total Environ*. 2013;458:140-149.
98. ICRP. Human respiratory tract model for radiological protection. *Annals of the ICRP 24*. ICRP Publication 66; 1994.
99. Salthammer T, Schripp T, Uhde E, Wensing M. Aerosols generated by hardcopy devices and other electrical appliances. *Environ Pollut*. 2012;169:167-174.
100. Salthammer T. Release of organic compounds and particulate matter from products, materials, and electrical devices in the indoor environment. In: Pluschke P, Schleibinger H, eds. *Indoor Air Pollution*, vol. 64. Springer Verlag; 2018:1-35.
101. Clausen PA, Liu Z, Kofoed-Sørensen V, Little J, Wolkoff P. Influence of temperature on the emission of di-(2-ethylhexyl)phthalate (DEHP) from PVC flooring in the emission cell FLEC. *Environ Sci Technol*. 2012;46:909-915.
102. Schwarzenbach RP, Gschwend PM, Imboden DM. *Environmental Organic Chemistry*. John Wiley & Sons; 2017.
103. Salthammer T, Morrison GC. Temperature and indoor environments. *Indoor Air*. 2022;32:e13022.
104. Singer BC, Hodgson AT, Hotchi T, et al. Sorption of organic gases in residential rooms. *Atmos Environ*. 2007;41:3251-3265.
105. Uhde E, Salthammer T. Influence of molecular parameters on the sink effect in test chambers. *Indoor Air*. 2006;16:158-165.
106. Tichenor BA, Guo Z, Dunn JE, Sparks LE, Mason MA. The interaction of vapour phase organic compounds with indoor sinks. *Indoor Air*. 1991;1:23-35.
107. Tichenor BA. ed *Characterising Sources of Indoor Air Pollution and Related Sink Effects*. American Society for Testing and Materials; 1996; No. STP 1287.
108. Lai ACK, Nazaroff WW. Modeling indoor particle deposition from turbulent flow onto smooth surfaces. *J Aerosol Sci*. 2000;31:463-476.
109. Hinds WC. *Aerosol Technology*, 2nd ed. John Wiley & Sons; 1999.
110. Atkinson R, Arey J. Atmospheric degradation of volatile organic compounds. *Chem Rev*. 2003;103:4605-4638.
111. Hoskovec M, Grygarová D, Cvačka J, et al. Determining the vapour pressures of plant volatiles from gas chromatographic retention data. *J Chromatogr A*. 2005;1083:161-172.
112. Emmerson KM, Carslaw N, Carslaw DC, et al. Free radical modelling studies during the UK TORCH Campaign in summer 2003. *Atmos Chem Phys*. 2007;7:167-181.
113. Hofzumahaus A, Aschmutat U, Brandenburger U, et al. Intercomparison of tropospheric OH measurements by different Laser techniques during the POPCORN campaign 1994. *J Atmos Chem*. 1998;31:227-246.
114. Sarwar G, Corsi R, Kimura Y, Allen D, Weschler CJ. Hydroxyl radicals in indoor environments. *Atmos Environ*. 2002;36:3973-3988.
115. Weschler CJ. Ozone in indoor environments: Concentration and chemistry. *Indoor Air*. 2000;10:269-288.
116. Weschler CJ, Shields HC. Production of the hydroxyl radical in indoor air. *Environ Sci Technol*. 1996;30:3250-3258.
117. Gligorovski S, Strekowski R, Barbati S, Vione D. Environmental Implications of Hydroxyl Radicals (•OH). *Chem Rev*. 2015;115:13051-13092.
118. Nørgaard AW, Nøjgaard JK, Larsen K, et al. Secondary limonene endo-ozonide: A major product from gas-phase ozonolysis of R-(+)-limonene at ambient temperature. *Atmos Environ*. 2006;40:3460-3466.

119. Coleman BK, Lunden MM, Destaillats H, Nazaroff WW. Secondary organic aerosol from ozone-initiated reactions with terpene-rich household products. *Atmos Environ*. 2008;42:8234-8245.
120. Arata C, Zarzana KJ, Misztal PK, et al. Measurement of NO_3 and N_2O_5 in a residential kitchen. *Environ Sci Technol Letters*. 2018;5:595-599.
121. Bidleman TF, Harner T. Sorption to Aerosols. In: Boethling RS, Mackay D, eds. *Handbook of Property Estimation Methods for Chemicals*. Lewis Publishers; 2000:233-260.
122. Baskaran S, Duan Lei Y, Wania F. Reliable prediction of the octanol-air partition ratio. *Environ Toxicol Chem*. 2021;40:3166-3180.
123. Rodgers TFM, Okeme JO, Parnis JM, et al. Novel Bayesian method to derive final adjusted values of physicochemical properties: Application to 74 compounds. *Environ Sci Technol*. 2021;55:12302-12316.
124. Liu C, Shi S, Weschler C, Zhao B, Zhang Y. Analysis of the dynamic interaction between SVOCs and airborne particles. *Aerosol Sci Technol*. 2013;47:125-136.
125. Weschler CJ, Nazaroff WW. Semivolatile organic compounds in indoor environments. *Atmos Environ*. 2008;42:9018-9040.
126. Weschler CJ, Nazaroff WW. Dermal uptake of organic vapors commonly found in indoor air. *Environ Sci Technol*. 2014;48:1230-1237.
127. Licina D, Morrison GC, Bekö G, Weschler CJ, Nazaroff WW. Clothing-mediated exposures to chemicals and particles. *Environ Sci Technol*. 2019;53:5559-5575.
128. Antretter F, Pazold M, Künzel HM, Sedlbauer KP. Anwendung hygrothermischer Gebäudesimulation. *Bauphysik Kalender 2015: Simulations-und Berechnungsverfahren*. 2015;189-225.

How to cite this article: Salthammer T, Zhao J, Schieweck A, et al. A holistic modeling framework for estimating the influence of climate change on indoor air quality. *Indoor Air*. 2022;32:e13039. doi:10.1111/ina.13039